Electronic Supplemental Materials (ESM):

ESM Tables:

ESM Table 1. Antibodies used for murine flow cytometry.

Target	Clone	Host	Fluorochrome	Concentration	Vendor	RRID
CD4	GK1.5	Rat	PerCP-Cy5.5	0.2 µg/mL	BioLegend	AB_893324
CD4	RM4-5	Rat	PE-Cy7	0.2 µg/mL	BioLegend	AB_312729
CD8α	53-6.7	Rat	BV711	0.06 µg/mL	BioLegend	AB_2562100
CD16/CD32	2.4G2	Rat	N/A	2 µg/mL	BD Pharmingen	AB_394656
CD25	PC61	Rat	APC	0.4 µg/mL	BioLegend	AB_493709
CD44	IM7	Rat	PE	0.4 µg/mL	BioLegend	AB_312959
CD62L	MEL-14	Rat	APC	0.4 µg/mL	BioLegend	AB_313099
CD226	TX42.1	Rat	BV650	0.4 µg/mL	BioLegend	AB_2716083
Foxp3	FJK-16s	Rat	AF488	0.8 µg/mL	eBioScience	AB_763537
Helios	22F6	Armenian Hamster	Pacific Blue	0.8 µg/mL	BioLegend	AB_10690535
Ki-67	16A8	Rat	PE-Cy7	0.8 µg/mL	BioLegend	AB_2632694
NKp46	29A1.4	Rat	AF647	0.4 µg/mL	BioLegend	AB_2563660
p-STAT5	C71E5	Rabbit	AF647	0.4 µg/mL	Cell Signaling	AB_2302702
Rat IgG2a	MRG2a-83	Mouse	FITC	0.4 µg/mL	BioLegend	AB_492924

ESM Table 2. Antibodies used for CITE-seq Staining.

Target	Clone	Host	Barcode	Concentration	Vendor	RRID
CD4	RM4-5	Rat	AACAAGACCCTTGAG	10 µg/mL	BioLegend	AB_2813913
CD8α	53-6.7	Rat	TACCCGTAATAGCGT	10 µg/mL	BioLegend	AB_2819776
CD16/CD32	S17011E	Rat	N/A	12.5 µg/mL	BioLegend	AB_2783138
CD44	IM7	Rat	TGGCTTCAGGTCCTA	10 µg/mL	BioLegend	AB_2813930
CD62L	MEL-14	Rat	TGGGCCTAAGTCATC	10 µg/mL	BioLegend	AB_2819800
TIGIT	1G9	Mouse	GAAAGTCGCCAACAG	10 µg/mL	BioLegend	AB_2819886

ESM Table 3. Differentially Expressed Genes in NOD pLN Between Anti-CD226 and Isotype Treatments.

ESM Table 4. Differentially Expressed Genes in NOD Pancreas Between Anti-CD226 and Isotype Treatments.

ESM Table 5. Differentially Expressed Genes Between Clusters for NOD Pancreas and pLN.

14 **ESM Figures:**

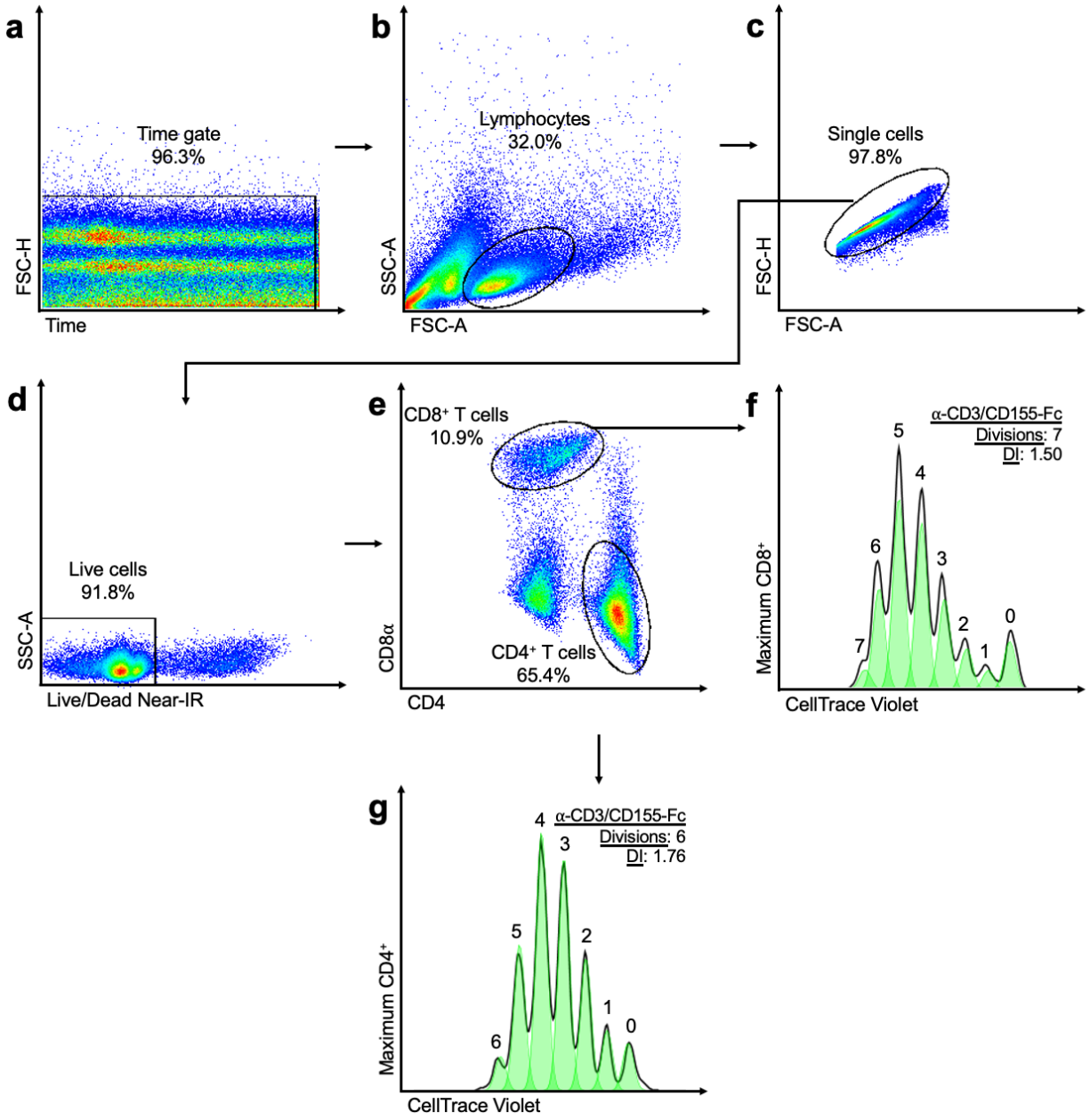

15

ESM Fig. 1. Gating Strategy for *In Vitro* Proliferation Assays.

Representative flow plots demonstrate how splenic $CD4^+$ T cells and $CD8^+$ T cells were identified for evaluating *in vitro* proliferation following treatment with isotype control or anti-CD226 mAb using a Cytek Aurora 5L Spectral Flow Cytometer. (**a**) Cells collected within a stable flow stream were gated using a time by forward scatter height (FSC-H) plot. (**b**) Lymphocyte gating was accomplished using forward scatter area (FSC-A) by side scatter area (SSC-A). (**c**) Single cells were gated upon using FSC-A by FSC-H. (**d**) Live lymphocytes were identified using a Live/Dead Near-IR dye exclusion. (**e**) Single-positive $CD4^+$ and $CD8^+$ T cell subsets within the live population were gated, before evaluating CellTrace Violet dye dilution, which was used to assess (**f**) $CD8^+$ and (**g**) $CD4^+$ Tresp proliferation after 4 days of co-culture with Tregs.

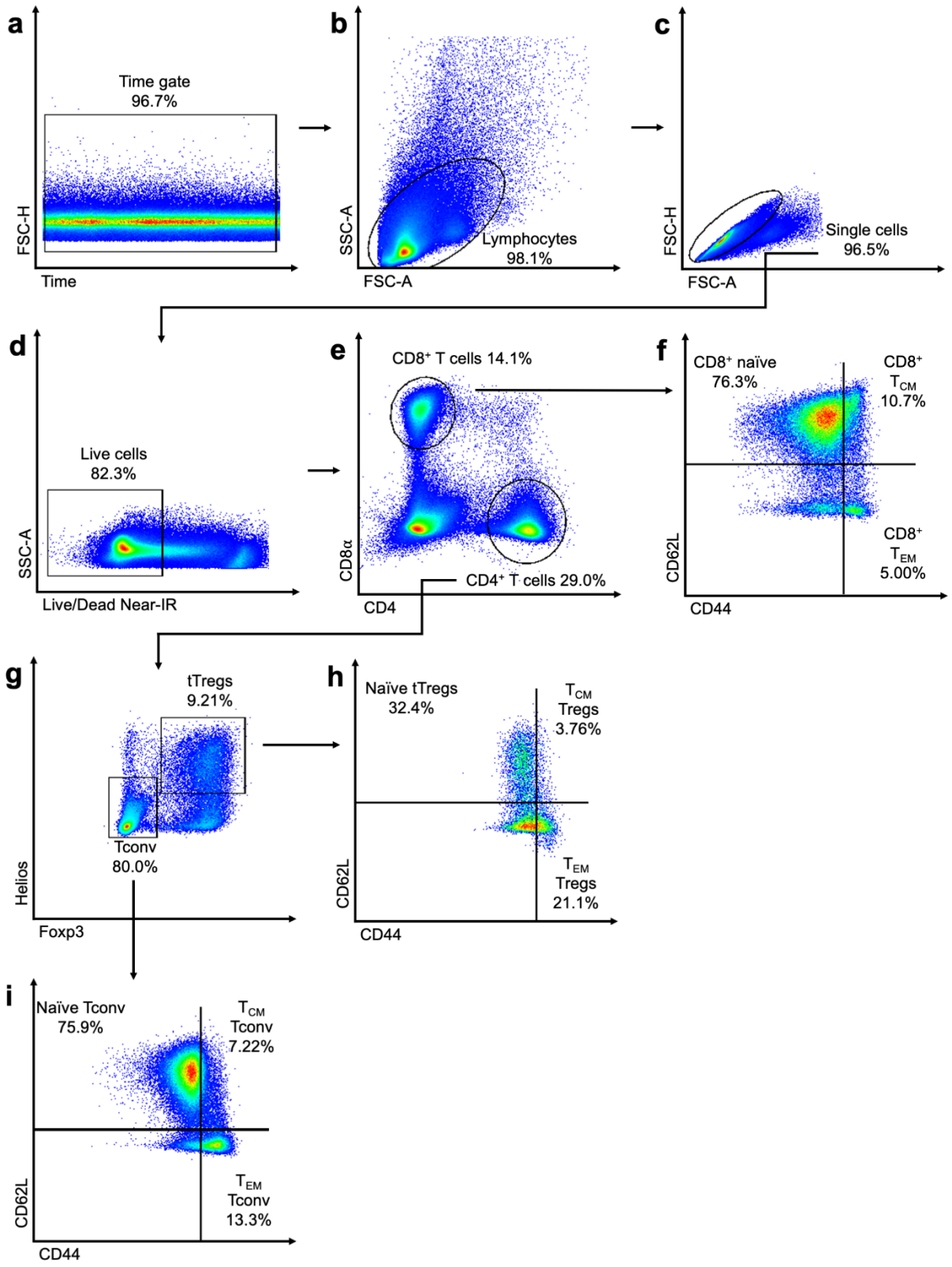
a
Time gate
96.7%
FSC-H
Time
b
SSC-A
Lymphocytes
98.1%
FSC-A
c
FSC-H
Single cells
96.5%
FSC-A
d
Live cells
82.3%
SSC-A
Live/Dead Near-IR
e
CD8⁺ T cells 14.1%
CD8α
CD4⁺ T cells 29.0%
CD4
f
CD8⁺ naïve
76.3%
CD8⁺
T_CM
10.7%
CD8⁺
T_EM
5.00%
CD62L
CD44
g
tTregs
9.21%
Tconv
80.0%
Helios
Foxp3
h
Naïve tTregs
32.4%
T_CM
Tregs
3.76%
T_EM
Tregs
21.1%
CD62L
CD44
i
Naïve Tconv
75.9%
T_CM
Tconv
7.22%
T_EM
Tconv
13.3%
CD62L
CD44

ESM Fig. 2. Gating Strategy for tTreg and Memory T cell Subsets.

Representative flow plots demonstrate how thymic Tregs (tTregs) and T cell memory subsets were defined for T cell immunophenotyping following treatment with isotype control or anti-CD226 mAb using a Cytek Aurora 5L Spectral Flow Cytometer. (**a**) Cells collected within a stable flow stream were gated using a time by forward scatter height (FSC-H) plot. (**b**) Lymphocyte gating was accomplished using forward scatter area (FSC-A) by side scatter area (SSC-A). (**c**) Single cells were gated upon using FSC-A by FSC-H. (**d**) Live lymphocytes were identified using a Live/Dead Near-IR dye exclusion to dying cells. (**e**) Single-positive $CD4^+$ and $CD8^+$ T cell subsets within the live population were gated before defining (**f**) $CD8^+$ Naïve ($CD44^-CD62L^+$), T central Memory (T_{CM}; $CD44^+CD62L^+$), and T effector Memory (TEM; $CD44^+CD62L^-$) cells using a CD44 by CD62L plot. (**g**) $CD4^+$ T cells were further defined as $Foxp3^-Helios^-$ Tconv or $Foxp3^+Helios^+$ tTregs, before identifying (**h**) $CD4^+$ tTreg and (**i**) Tconv memory subsets using CD44 by CD62L plots, as previously described.

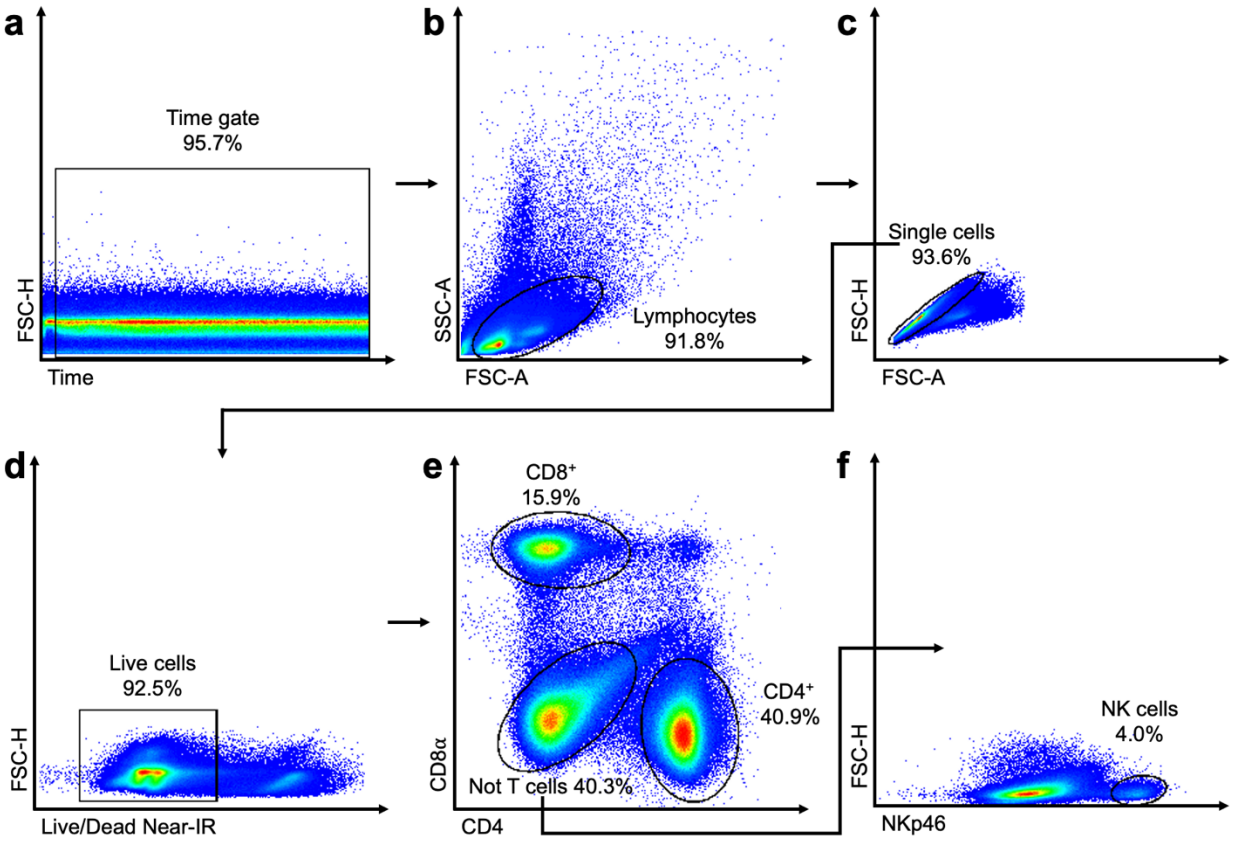

ESM Fig. 3. Gating Strategy for Detection of anti-CD226 (Clone 480.1) Blocking Antibody. Representative flow plots demonstrate how splenic $CD4^+$ T cells, $CD8^+$ T cells, and natural killer (NK) cells were defined for evaluating *in vivo* persistence of anti-CD226 mAb using a Cytek Aurora 5L Spectral Flow Cytometer. (**a**) Cells collected within a stable flow stream were gated using a time by forward scatter height (FSC-H) plot. (**b**) Lymphocyte gating was accomplished using forward scatter area (FSC-A) by side scatter area (SSC-A). (**c**) Single cells were gated upon using FSC-A by FSC-H. (**d**) Live lymphocytes were identified using a Live/Dead Near-IR dye exclusion. (**e**) Single-positive $CD4^+$ and $CD8^+$ T cell subsets within the live population were gated, whereas (**f**) NK receptor-expressing cells were defined as $CD4^-CD8^-$ lymphocytes expressing NKp46.

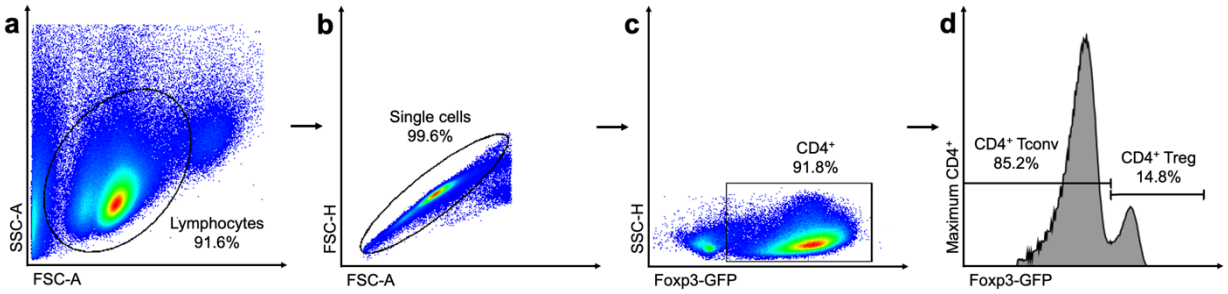

ESM Fig. 4. Fluorescence Activated Cell Sorting (FACS) Isolation Strategy for CD4$^+$ Tconv and Tregs.

Representative flow plots demonstrate how splenic CD4$^+$ Tconv and Tregs were isolated for *in vitro* suppression assays using a BD FACSMelody Cell Sorter. (**a**) Lymphocyte gating was accomplished using forward scatter area (FSC-A) by side scatter area (SSC-A). (**b**) Single cells were gated upon using FSC-A by forward scatter height (FSC-H). (**c**) CD4$^+$ T cells were gated before defining (**d**) GFP$^+$ Tregs and GFP$^-$ Tconv using the Foxp3-GFP reporter.

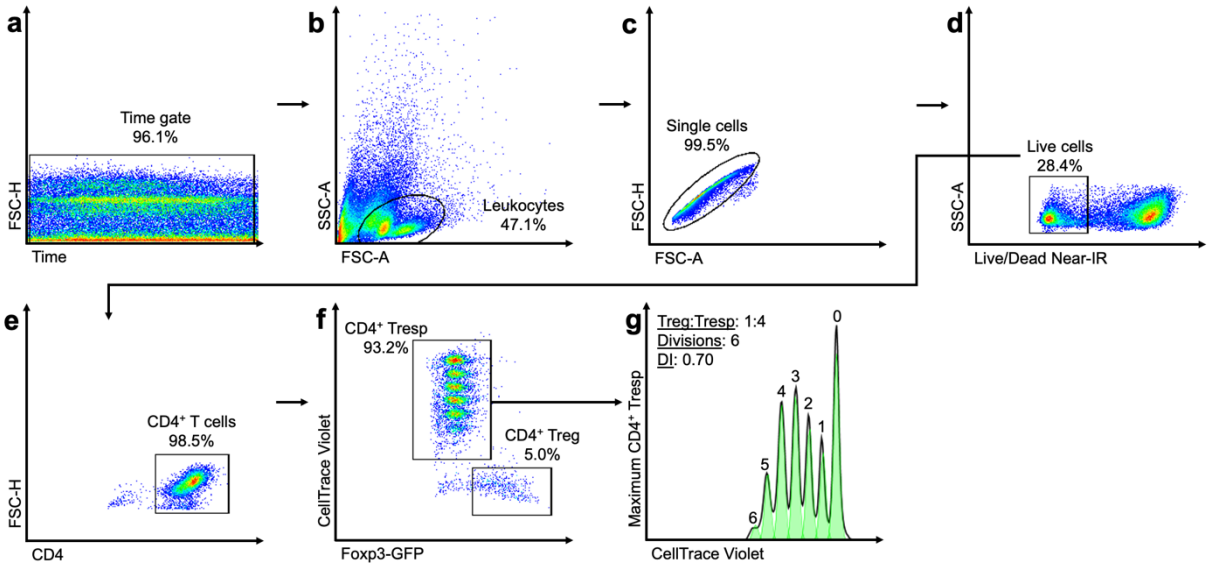

ESM Fig. 5. Gating Strategy for Assessing *In Vitro* Suppression of CD4$^+$ Tresp. Representative flow plots demonstrate how splenic CD4$^+$ T cells, CD8$^+$ T cells, and natural killer (NK) cells were defined for evaluating *in vivo* persistence of anti-CD226 mAb using a Cytek Aurora 5L Spectral Flow Cytometer. (**a**) Cells collected within a stable flow stream were gated using a time by forward scatter height (FSC-H) plot. (**b**) Leukocyte gating was accomplished using forward scatter area (FSC-A) by side scatter area (SSC-A). (**c**) Single cells were gated using FSC-A by FSC-H. (**d**) Live leukocytes were identified using a Live/Dead Near-IR dye exclusion. (**e**) CD4$^+$ T cells within the live population were gated before defining (**f**) CellTrace Violet (CTV)$^-$ GFP$^+$ Tregs and CTV$^+$GFP$^-$ Tresp. (**g**) CTV dye dilution was used to assess Tresp proliferation after four days of co-culture with Tregs.

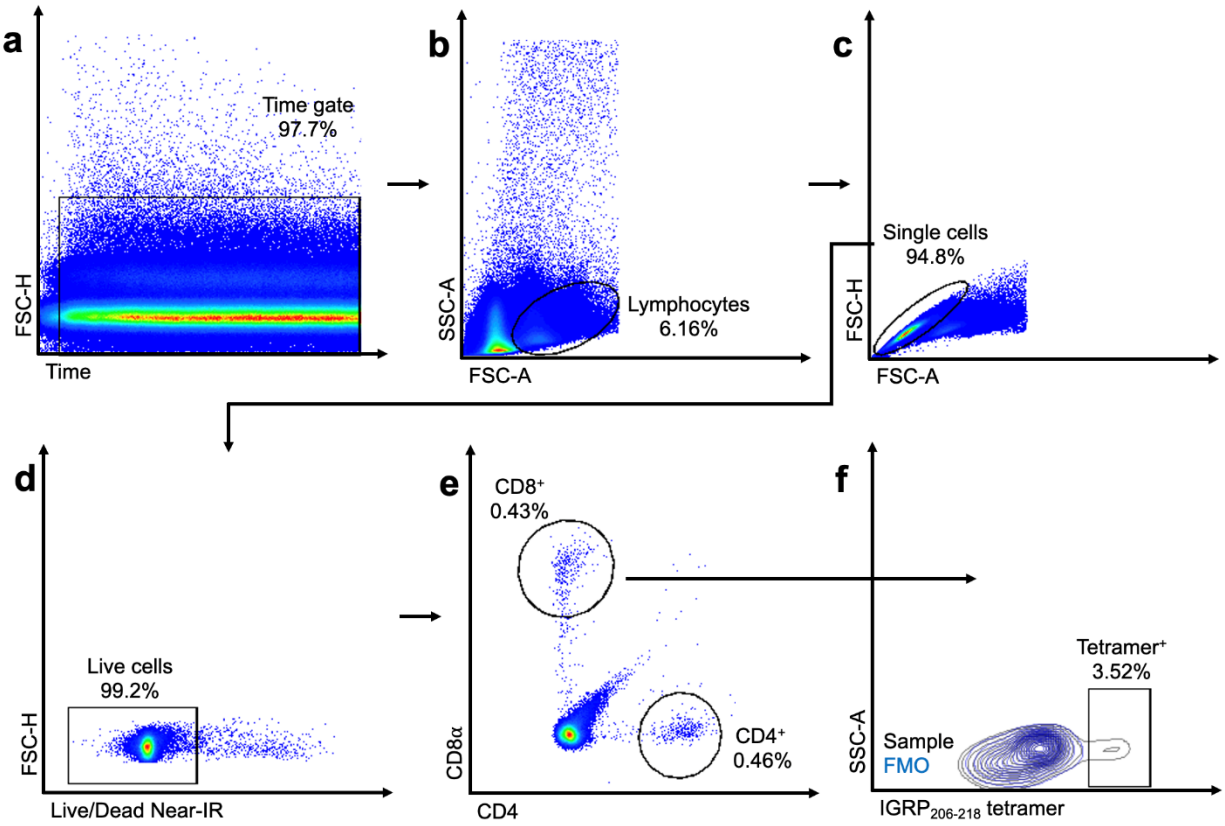

ESM Fig. 6. Gating Strategy for IGRP$_{206-218}$ Tetramer Staining.

Representative flow plots demonstrate how IGRP-reactive pancreatic CD8$^+$ T cells were defined using a Cytek Aurora 5L Spectral Flow Cytometer. (**a**) Cells collected within a stable flow stream were gated using a time by forward scatter height (FSC-H) plot. (**b**) Lymphocyte gating was accomplished using forward scatter area (FSC-A) by side scatter area (SSC-A). (c) Single cells were gated upon using FSC-A by FSC-H. (**d**) Live lymphocytes were identified using a Live/Dead Near-IR dye exclusion. (**e**) Single-positive CD4$^+$ and CD8$^+$ T cell subsets within the live population were gated before defining (**f**) IGRP$_{206-218}$ tetramer-positive CD8$^+$ T cells (black) using a fluorescence minus one (FMO) control (blue).

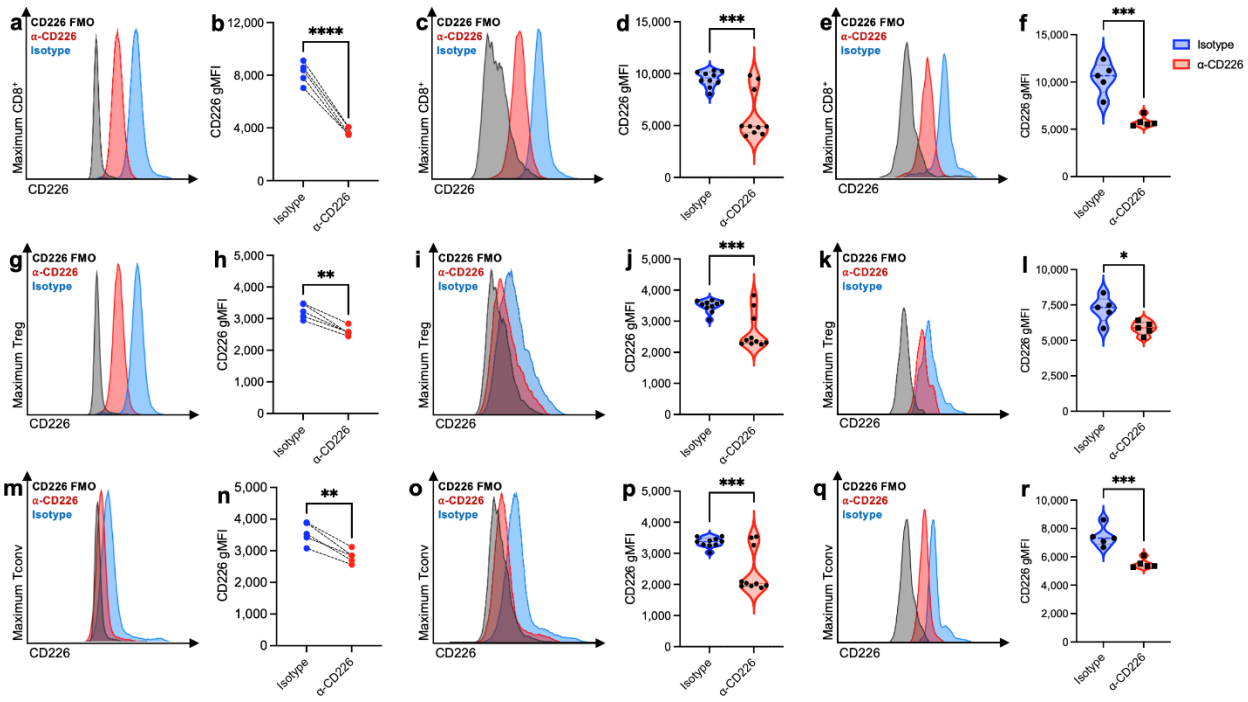

ESM Fig. 7. CD226 Accessibility is Reduced Following anti-CD226 mAb Treatment.

The accessibility of CD226 on $CD8^+$ T cells (**a-f**), $CD4^+$ Tregs (**g-l**), and $CD4^+$ Tconv (**m-r**) obtained from NOD spleens or pancreata was assessed using flow cytometry following either *in vitro* (**a-b, g-h, m-n,** biological n=5) or five weeks following *in vivo* (spleen: **c-d, i-j, o-p,** biological n=10; pancreas: **e-f, k-l, q-r,** biological n=5) treatment with either IgG2a isotype control (blue) or anti-CD226 clone 480.1 (red). Representative histograms show staining with BV650-conjugated anti-CD226 clone TX42.1 (**a, c, e, g, i, k, m, o, q**) relative to CD226 fluorescence minus one (FMO) controls (black), with paired dot or violin plots showing the gMFI of CD226 (**b, d, f, h, j, l, n, p, r**). Significant p-values are reported for t-tests of paired *in vitro* samples and unpaired *ex vivo* samples between treatment conditions. *p<0.05, **p<0.01, ***p<0.001, ****p<0.0001.

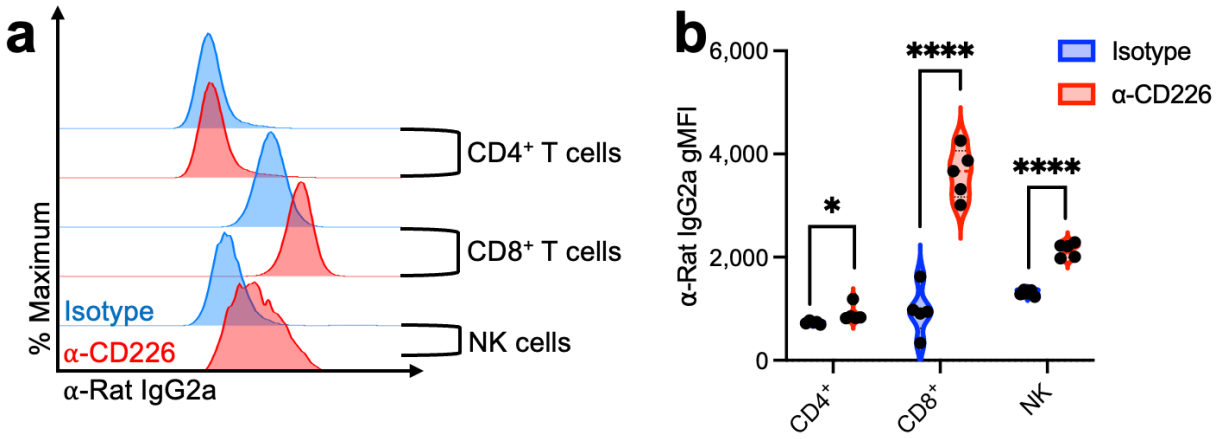

ESM Fig. 8. Anti-CD226 mAb Persist *In Vivo* for At Least Five Weeks.

Five weeks following *in vivo* treatment with anti-CD226 clone 480.1 mAb (red) or rat IgG2a isotype control (blue), splenocytes were stained with a FITC-labeled α-rat IgG2a mAb to detect cell-bound anti-CD226 or isotype control on three subsets known to express CD226: $CD4^+$ T cells, $CD8^+$ T cells, and NK cells, as shown in (**a**) Representative histograms and (**b**) violin plots (biological n=5/condition). Significant p-values are reported on the figure for unpaired t-tests for each cell subset between treatment conditions. *p=0.048, ****p<0.0001.

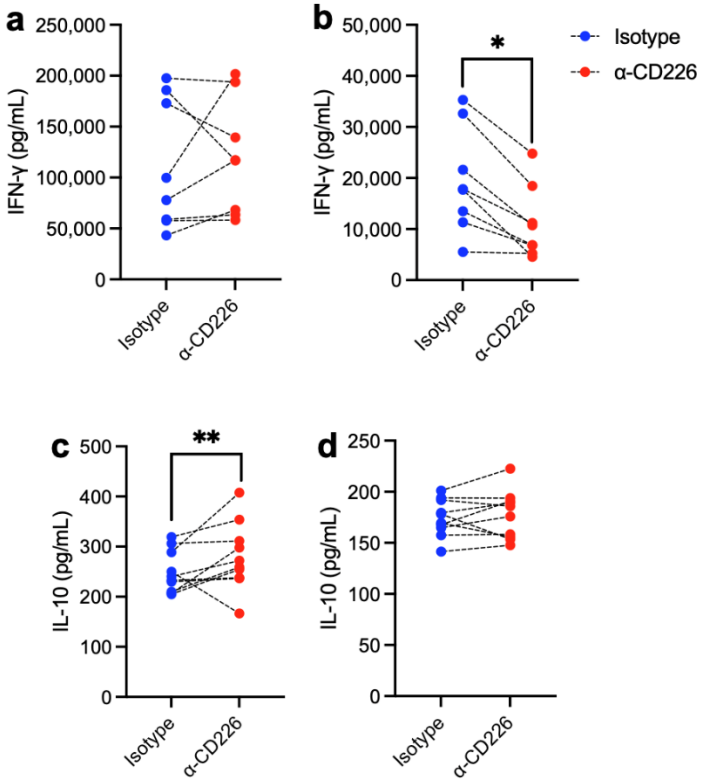

ESM Fig. 9. Anti-CD226 mAb Blockade Alters T Cell Cytokine Production.

To assess the impact of anti-CD226 mAb blockade on (**a-b**) IFN-γ and (**c-d**) IL-10 cytokine secretion, cell culture supernatants from splenocytes incubated with IgG2a isotype control (blue) or anti-CD226 mAb (red), then stimulated *in vitro* with either (**a, c**) α-CD3/α-CD28 or (**b, d**) α-CD3/CD155-Fc were analyzed by ELISA. Data reflects biological n=8/condition. Paired dot plots show significant p-values reported for two-way ANOVA with Bonferroni correction for multiple comparisons. *p=0.025, **p=0.0040.

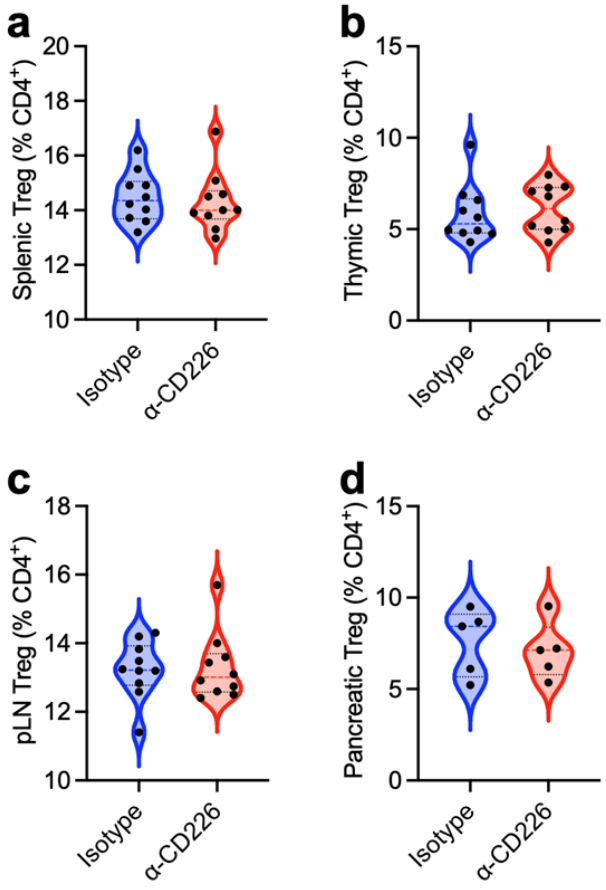

ESM Fig. 10. Treatment of NOD mice with anti-CD226 mAb Does Not Impact Treg Frequency.

Violin plots show the frequencies of $CD4^+$ Tregs in the (**a**) spleen, (**b**) thymus, (**c**) pancreatic-draining lymph nodes (pLN) (n=10/treatment group), and (**d**) pancreas (n=5/treatment group), five weeks following treatment with isotype or anti-CD226. No significant p-values were identified for differences in Treg frequency using paired T tests.

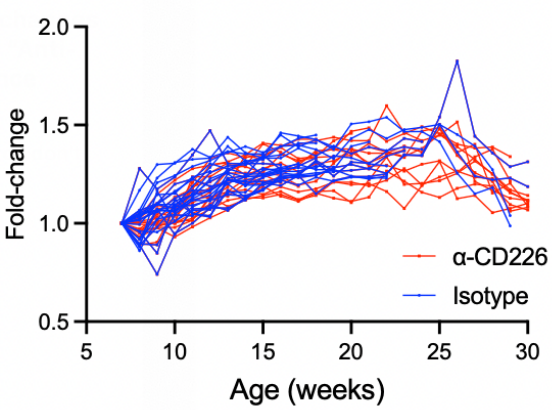

ESM Fig. 11. Treatment of NOD mice with anti-CD226 mAb Does Not Impact Body Mass. Female NOD mice were treated with either IgG2a isotype control (blue) or anti-CD226 mAb (red) and monitored weekly until diabetes onset or 30 weeks of age. Spaghetti plots show fold change in weight from pre-treatment mass at seven weeks of age through the study endpoint. Data reflects biological n=2-25/treatment group at each time point. No significant p-values were identified for changes in mass using Mixed Effects Analysis with Bonferroni correction for multiple comparisons between treatment conditions.

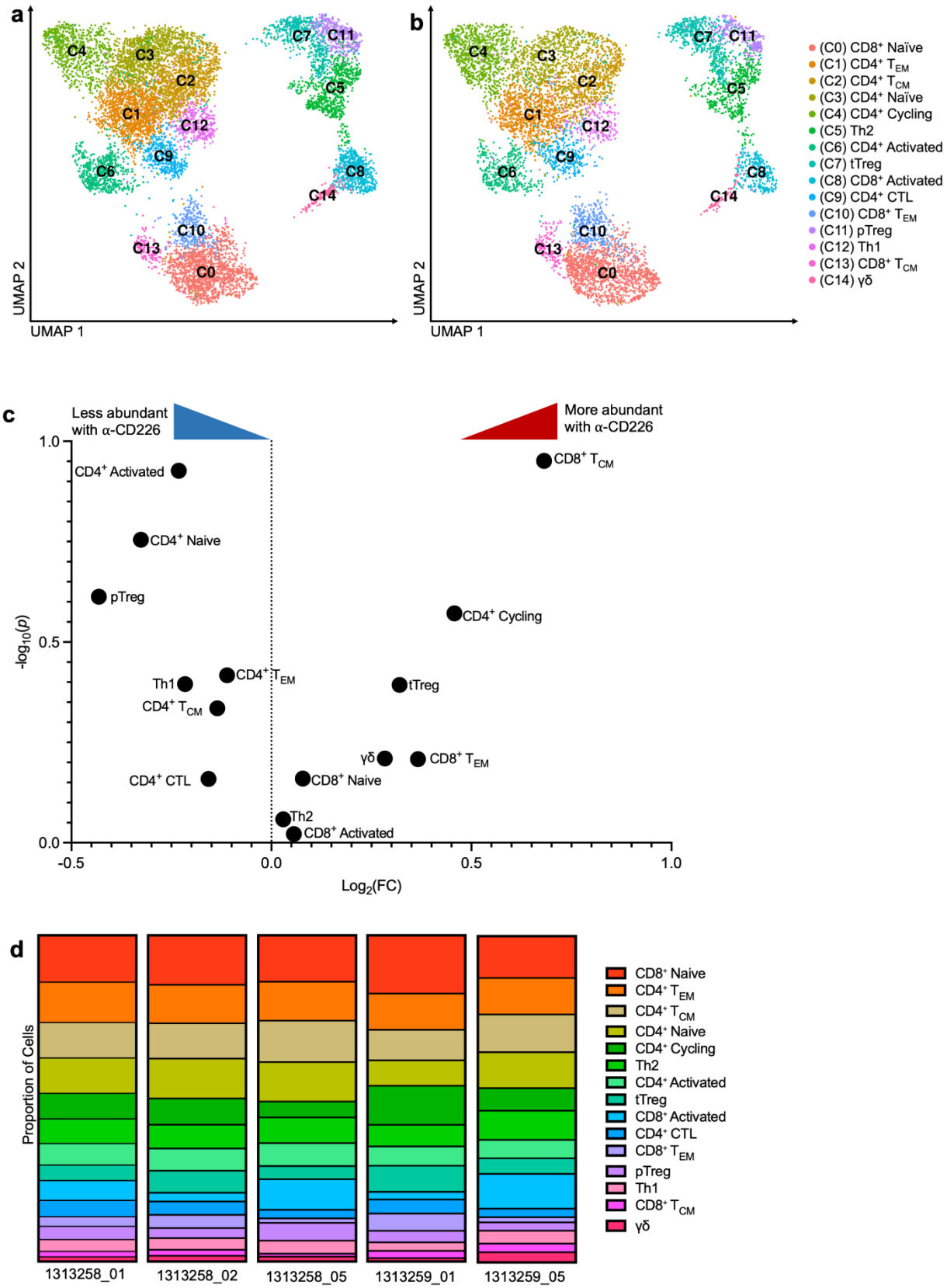
a
b
UMAP 1
UMAP 2
C0
C1
C2
C3
C4
C5
C6
C7
C8
C9
C10
C11
C12
C13
C14
(C0) CD8⁺ Naïve
(C1) CD4⁺ T_EM
(C2) CD4⁺ T_CM
(C3) CD4⁺ Naïve
(C4) CD4⁺ Cycling
(C5) Th2
(C6) CD4⁺ Activated
(C7) tTreg
(C8) CD8⁺ Activated
(C9) CD4⁺ CTL
(C10) CD8⁺ T_EM
(C11) pTreg
(C12) Th1
(C13) CD8⁺ T_CM
(C14) γδ
c
Less abundant with α-CD226
More abundant with α-CD226
CD4⁺ Activated
CD4⁺ Naive
pTreg
Th1
CD4⁺ T_EM
CD4⁺ T_CM
CD4⁺ CTL
Th2
CD8⁺ Activated
CD8⁺ Naive
γδ
CD8⁺ T_EM
tTreg
CD4⁺ Cycling
CD8⁺ T_CM
-log10(p)
Log2(FC)
d
Proportion of Cells
1313258_01
1313258_02
1313258_05
1313259_01
1313259_05
CD8⁺ Naive
CD4⁺ T_EM
CD4⁺ T_CM
CD4⁺ Naive
CD4⁺ Cycling
Th2
CD4⁺ Activated
tTreg
CD8⁺ Activated
CD4⁺ CTL
CD8⁺ T_EM
pTreg
Th1
CD8⁺ T_CM
γδ

ESM Fig. 12. Anti-CD226 mAb Does Not Impact Pancreatic T cell Cluster Abundance.

A differential abundance analysis was performed on T cell clusters identified in the pancreas of 12-week-old female NOD mice five weeks after treatment with anti-CD226 mAb or isotype control. UMAP projections show the abundance of annotated T cell clusters in the pancreata of (**a**) isotype and (**b**) anti-CD226 treated mice. (**c**) The volcano plot shows differential abundance values for each T cell cluster with the -log10(p-value) determined by gene-wise negative binomial generalized linear models. (**d**) Stacked bar plots show the proportion of each subset, with each T cell cluster represented similarly between samples.

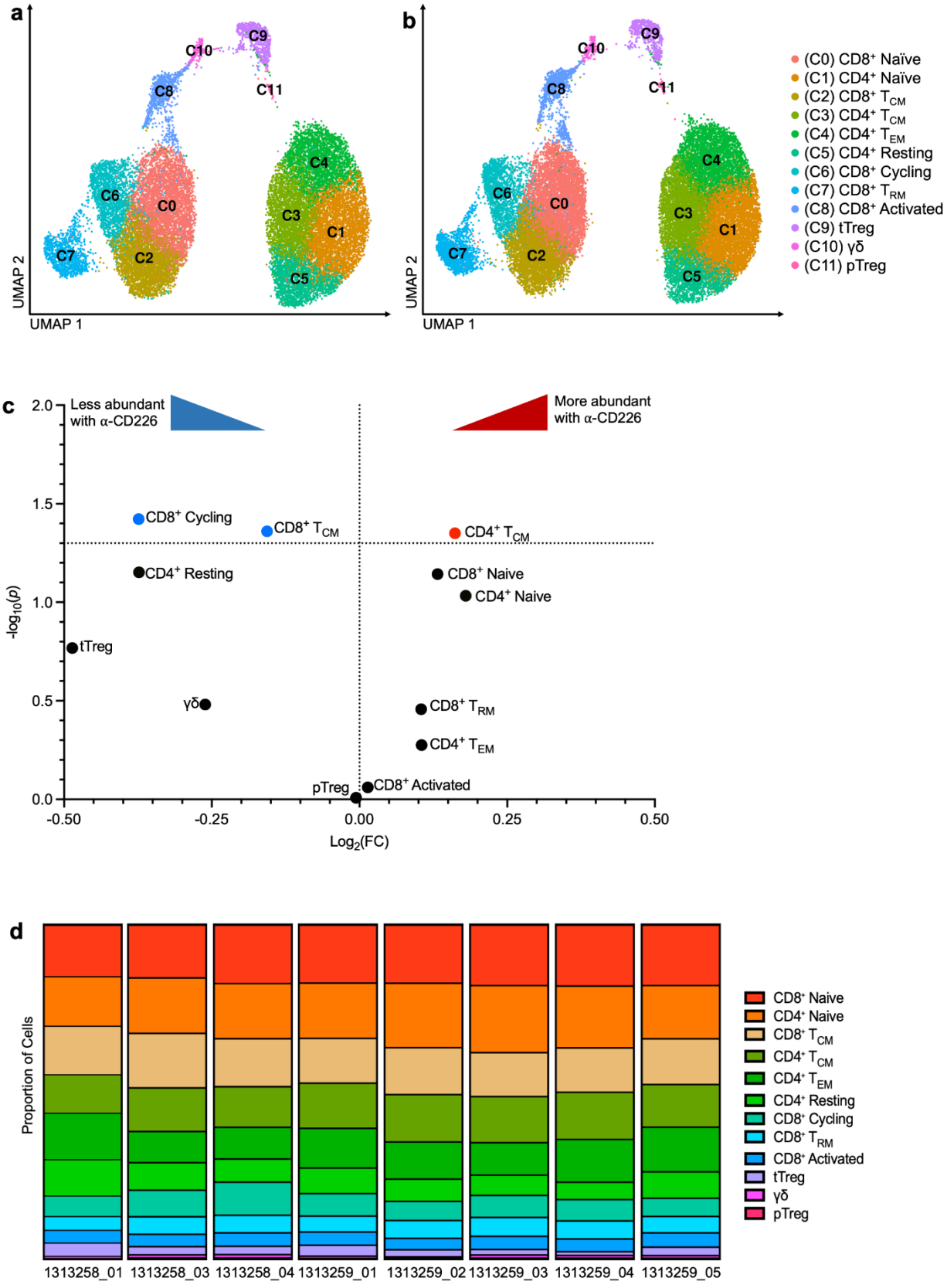
a
b
C0
C1
C2
C3
C4
C5
C6
C7
C8
C9
C10
C11
UMAP 1
UMAP 2
(C0) CD8⁺ Naïve
(C1) CD4⁺ Naïve
(C2) CD8⁺ TCM
(C3) CD4⁺ TCM
(C4) CD4⁺ TEM
(C5) CD4⁺ Resting
(C6) CD8⁺ Cycling
(C7) CD8⁺ TRM
(C8) CD8⁺ Activated
(C9) tTreg
(C10) γδ
(C11) pTreg
c
Less abundant with α-CD226
More abundant with α-CD226
CD8⁺ Cycling
CD8⁺ TCM
CD4⁺ TCM
CD4⁺ Resting
CD8⁺ Naive
CD4⁺ Naive
tTreg
γδ
CD8⁺ TRM
CD4⁺ TEM
pTreg
CD8⁺ Activated
-log10(p)
Log2(FC)
d
Proportion of Cells
1313258_01
1313258_03
1313258_04
1313259_01
1313259_02
1313259_03
1313259_04
1313259_05
CD8⁺ Naive
CD4⁺ Naive
CD8⁺ TCM
CD4⁺ TCM
CD4⁺ TEM
CD4⁺ Resting
CD8⁺ Cycling
CD8⁺ TRM
CD8⁺ Activated
tTreg
γδ
pTreg

ESM Fig. 13. Anti-CD226 mAb Blockade May Alter T Cell Priming and Memory Differentiation in the Pancreatic Lymph Node (pLN).

A differential abundance analysis was performed on T cell clusters identified in the pLN from 12-week-old female NOD mice five weeks after treatment with anti-CD226 mAb or isotype control. UMAP projections show the abundance of annotated T cell clusters in pLN of (**a**) isotype and (**b**) anti-CD226 treated mice. (**c**) The volcano plot shows differential abundance values for each T cell cluster with the -log10(p-value) determined by gene-wise negative binomial generalized linear models. (**d**) Stacked bar plots show the proportion of each subset, with each T cell cluster represented similarly between samples.

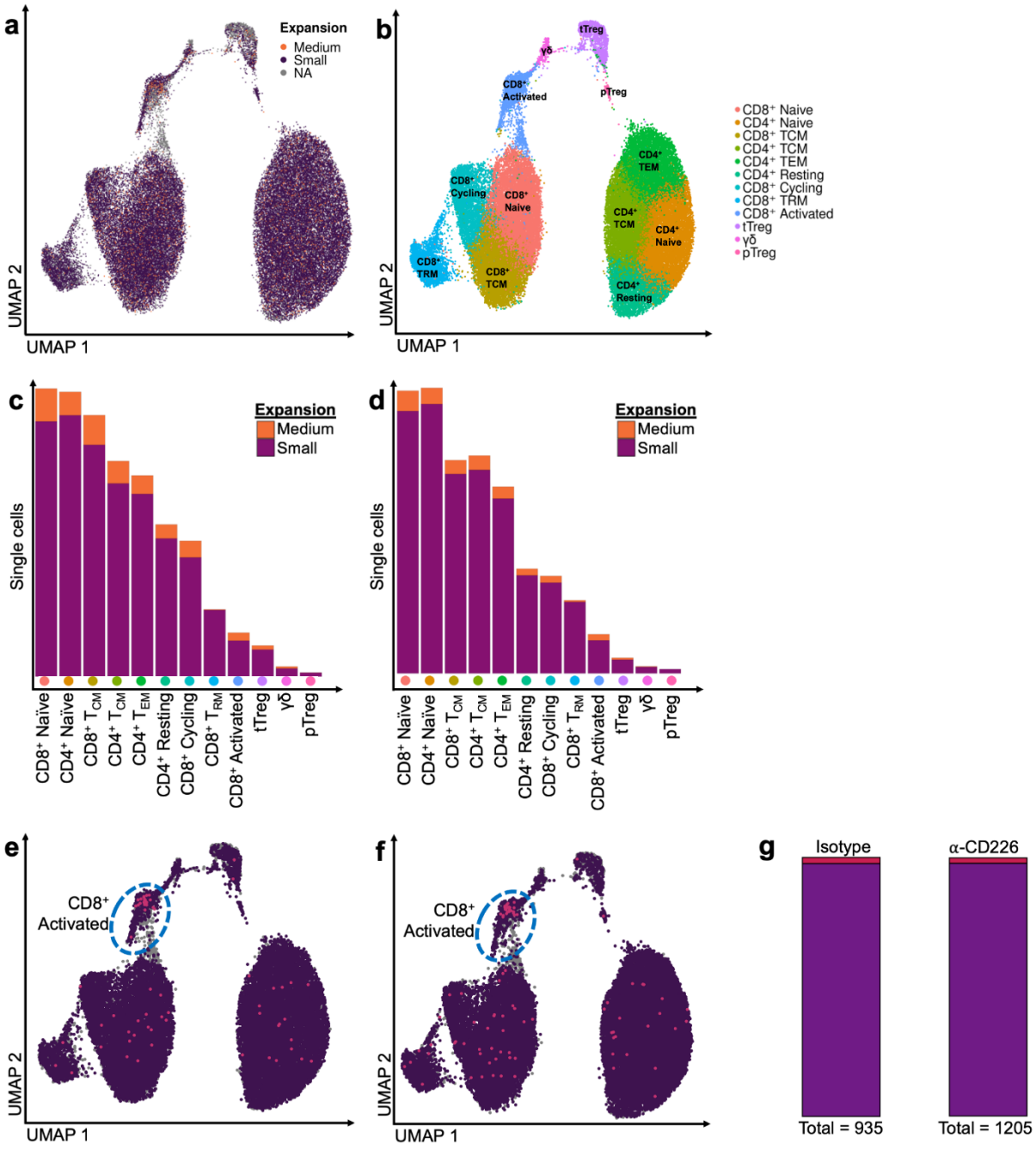
a
Expansion
Medium
Small
NA
UMAP 2
UMAP 1
b
tTreg
γδ
CD8⁺ Activated
pTreg
CD4⁺ TEM
CD8⁺ Cycling
CD8⁺ Naive
CD4⁺ TCM
CD4⁺ Naive
CD8⁺ TRM
CD8⁺ TCM
CD4⁺ Resting
CD8⁺ Naive
CD4⁺ Naive
CD8⁺ TCM
CD4⁺ TCM
CD4⁺ TEM
CD4⁺ Resting
CD8⁺ Cycling
CD8⁺ TRM
CD8⁺ Activated
tTreg
γδ
pTreg
c
Expansion
Medium
Small
Single cells
CD8⁺ Naïve
CD4⁺ Naïve
CD8⁺ TCM
CD4⁺ TCM
CD4⁺ TEM
CD4⁺ Resting
CD8⁺ Cycling
CD8⁺ TRM
CD8⁺ Activated
tTreg
γδ
pTreg
d
Expansion
Medium
Small
Single cells
CD8⁺ Naïve
CD4⁺ Naïve
CD8⁺ TCM
CD4⁺ TCM
CD4⁺ TEM
CD4⁺ Resting
CD8⁺ Cycling
CD8⁺ TRM
CD8⁺ Activated
tTreg
γδ
pTreg
e
CD8⁺ Activated
UMAP 2
UMAP 1
f
CD8⁺ Activated
UMAP 2
UMAP 1
g
Isotype
α-CD226
Total = 935
Total = 1205

ESM Fig. 14. Anti-CD226 mAb Blockade Does Not Alter T Cell Clonal Expansion in the Pancreatic Lymph Node (pLN).

To determine the impact of anti-CD226 mAb blockade on T cell clonal expansion in the pLN, TCR-seq data from each cell was merged with corresponding scRNA-seq data. (**a**) The degree of clonal expansion within each cluster was assessed by overlaying the proportion of each clonotype (Medium: $0.001 < X < 0.01$ (orange), Small: $1e^{-4} < X < 0.001$ (pink), NA: no CDR3 sequence for cell barcode (gray)) onto a Uniform Manifold Approximation and Projection (UMAP) of T cells isolated from NOD pLN, five weeks following treatment. (**b**) UMAP plots annotated with distinct T cell clustering for the pLN (17,617 cells). Stacked bar plots show the distribution of clonal expansion by cluster in mice treated with (**c**) isotype (**d**) or anti-CD226. UMAP plots split by treatment condition show T cells containing CDR3 sequences within one amino acid of previously published IGRP-reactive clones (Kasmani *et al.*), annotated as IGRP-reactive (pink) or as having another reactivity (purple) from (**e**) isotype or (**f**) anti-CD226 treated mice. (**g**) Stacked bar plots show the frequency of IGRP-reactive clones within the $CD8^+$ Activated T cell cluster between isotype or anti-CD226 treated mice. No significant p-values were identified using Fisher's Exact Test between treatment conditions.